The Cryosphere Discuss., doi:10.5194/tc-2016-88, 2016
Manuscript under review for journal The Cryosphere
Published: 27 April 2016


The Cryosphere Discussions
Open Access
EGU

# Semi-brittle rheology and ice dynamics in DynEarthSol3D

Liz C. Logan[1], Luc L. Lavier[2, 3], Eunseo Choi[4], Eh Tan[5], Ginny A. Catania[2, 3]

[1]Institute for Computational and Engineering Science, University of Texas, Austin, 78712, USA
[2]Department of Geological Science, University of Texas, Austin, 78712, USA
[3]Institute for Geophysics, University of Texas, Austin, 78758, USA
[4]Center for Earthquake Research and Information, University of Memphis, Memphis, 38152, USA
[5]Institute of Earth Sciences, Academia Sinica, Taipei, No. 128, Section 2, Taiwan

*Correspondence to*: Liz C. Logan (liz.curry.logan@gmail.com)

**Abstract.** We present a semi-brittle rheology and explore its potential for simulating glacier and ice sheet deformation using a numerical model DynEarthSol3D (DES). DES is a finite element solver for the dynamic and quasi-static simulation of continuous media. The experiments within demonstrate that DES can simulate ice failure and deformation in dynamic regions of glaciers, especially at quickly changing boundaries such as where glaciers meet the ocean. We explore the effect that different initial, boundary, and material conditions have on ice flow and failure. We find that the use of a semi-brittle constitutive law is a necessary material condition to form the characteristic pattern of basal crevasse-aided pinch-and-swell geometry, which is observed globally in floating portions of ice and can often aid in eroding the ice sheet margins in direct contact with oceans.

**Keywords:**

Numerical modeling, rheology, ice fracture, basal crevasses.

## 1 Introduction

Accurate prediction of global sea-level rise depends critically on numerical models' ability to project the removal of ice from the margins of ice sheets and glaciers under climate change scenarios – especially those in contact with oceans. In the past five years numerical models have largely risen to the challenge of simulating the continent-scale, steady state viscous flow of ice, leading to the development

The Cryosphere Discuss., doi:10.5194/tc-2016-88, 2016
Manuscript under review for journal The Cryosphere
Published: 27 April 2016




of the latest class of ice sheet models that represent ice physics across many flow regimes and in three spatial dimensions. These are often non-linearly viscous, thermo-mechanical models that solve the so-called full-Stokes (FS) equations (e.g., Gagliardini and Zwinger, 2008; Larour et al., 2012). Models based on shallow ice (SIA) and shallow shelf (SSA) approximations of the FS equations are also in wide use and simulate ice flow well in most areas (e.g. Winkelmann et al., 2011; Lipscomb et al., 2013). Regardless of their computational cores, most models are designed largely for steady state flow, or diagnostic execution; there are several widely used models designed to simulate prognostic, time-dependent ice flow (Martin et al., 2004; Gagliardini and Zwinger, 2008; Larour et al., 2012) and therefore specifically equipped to simulate ice retreat.

Despite recent advances many pertinent questions in glaciology remain that could potentially be addressed best from a computational perspective, particularly with regard to the representation of retreat at ice sheet margins (especially where ice is often in contact with warm ocean water), via a process called calving. However representing the smaller scale physics at the heart of this particular problem (i.e., the fracture of crystalline material) often imposes too large a computational cost to remain a tractable problem for many models. Thus both the FS and SIA/SSA formulations employ parametrizations for the most physically complicated aspects of their systems. In particular, the failure of ice within many ice sheet models is treated using Linear Elastic Fracture Mechanics (e.g., Larour et al., 2012), or sometimes as a rheologically more flexible, time-dependent scalar damage field (e.g., Duddu et al., 2012).

Ice rheology has been studied using both geophysical observations and laboratory experiments (Budd & Jacka, 1989; Sammonds et al., 1998; Goldsby and Kohlstedt, 2001; Mahrenholtz and Wu, 1992). Over short time scales ice behaves elastically before yielding or flowing viscously. Over long time scales ice behaves as a viscous fluid for which the viscosity is non-linearly dependent on both temperature and effective stress (Glen, 1955). The resulting constitutive law is called Glen's flow law in glaciological literature and can be written as:

$$\dot{\varepsilon_e} = A\sigma_e^n, \quad (1)$$

The Cryosphere Discuss., doi:10.5194/tc-2016-88, 2016
Manuscript under review for journal The Cryosphere
Published: 27 April 2016




where $A$ represents an Arrhenius temperature relation, $\dot{\varepsilon}_e$ is the effective strain rate (the square root of the second invariant of the full strain rate tensor), and $n$ is typically set to 3. Laboratory experiments also show that ice strain-rate hardens and that it starts to fracture in a brittle manner at high strain rate (Schulson and Duval, 2009). In nature, calving results from the fracture of ice and is a consequence of brittle or ductile deformation (van der Veen, 1998; Weiss, 2004). Ductile fracture is initiated by the formation of distributed voids that eventually coalesce to form a macroscopic fracture (seen for example in the Amery Ice Shelf, Bassis et al., 2008), and is a slow process for which weakening by voids occurs over a prolonged stress plateau. On the other hand, the breaking or damage process for brittle fractures occurs abruptly for a given value of stress and strain-rate (Sammonds et al., 1998; Schulson and Duval, 2009).

Most numerical models simulate the long-term (hundreds to thousands of years), large-scale behaviour of ice sheets using a non-linear viscous formulation to calculate the stress tensor (e.g., Larour et al., 2012). Indeed, for simulating long term flow of ice sheets this is an excellent approximation as the Maxwell viscoelastic stress relaxation timescale (time to dissipate elastic stresses) is on the order of a hours to days – depending on local material properties that affect the viscosity and shear modulus of ice (MacAyeal & Sergienko, 2013). These models may be less successful however when simulating the retreat of ice at marine terminating ice sheet margins on shorter time scales: the processes that lead to ice failure and ice retreat (which in turn modify the local stress field) are simply not represented as the stress field evolves through time. Because glacier retreat is ultimately related to ice fracture and calving, even those models that use Linear Elastic Fracture Mechanics as a yield criterion may not be evaluating the correct stresses if their rheology is assumed to be purely viscous. Often even simpler parameterizations are employed that prescribe margin position for termini in contact with ocean water, which depend empirically on strain rate fields derived from estimated viscous stresses (Levermann et al., 2012).

While it is true that the Maxwell viscoelastic relaxation time is on the order of hours to days, the need to consider elastic stress remains in ice modeling to simulate terminus retreat. This retreat depends on a long history of failure accumulation – accrued over time scales orders of magnitude larger than the Maxwell relaxation time – as well as a time-dependent forcing by the ocean on the floating ice (e.g.,

The Cryosphere Discuss., doi:10.5194/tc-2016-88, 2016
Manuscript under review for journal The Cryosphere
Published: 27 April 2016




Bindschadler et al., 2011). For example, calving via the detachment of large, tabular icebergs is an important end-member of observed calving styles (Amundsen and Truffer, 2010). The fractures that determine the size of very large icebergs—such as the 'loose tooth' at the terminus of the Amery Ice Shelf, and thus the calving rate in these locations – are exactly those features that result from brittle or ductile deformation over yearly to decadal time scales (Bassis et al., 2008). Thus while the elastic component of stress relaxes away over long-term simulations, the fractures resulting from the elastic component of stress remain and affect the dynamics of ice (e.g., the complete disintegration of the Larsen B Ice Shelf, examined by Glasser and Scambos, 2008).

In this paper we employ a Lagrangian finite element method that allows for both elastic and viscous component of ice deformation to be taken in to account, while simulating ice failure on unstructured meshes. We specifically explore how failure zones form and propagate in an advecting visco-elasto-plastic ice slab as it loses contact with the underlying bedrock and begins to float. The model exploration here is not meant to be wide-reaching and exhaustive; rather, it is presented as a tool to aid in the exploration of how the failure of ice impacts its flow.

## 2 Model description

DES (DynEarthSol3D) is a robust, adaptive, two- and three-dimensional finite element method that solves the momentum balance and heat equation in Lagrangian form using unstructured meshes.

### 2.1 Equations of motion

While many FS models neglect acceleration and formulate ice flow as a static problem, momentum conservation in DES takes the full dynamic form:

$$\rho \dot{\boldsymbol{u}} = \boldsymbol{\nabla} \cdot \boldsymbol{\sigma} + \rho \boldsymbol{g}, \tag{2}$$

where $\rho$ is the material density, $\boldsymbol{u}$ is the velocity vector, $\boldsymbol{\sigma}$ is the Cauchy stress tensor, and $\boldsymbol{g}$ is the acceleration due to gravity. The dot above $\boldsymbol{u}$ is the total time derivative, and variables in boldface are vectors or tensors. The $\nabla\cdot$ is the divergence operator. DES is designed to solve dynamic and quasi-static

The Cryosphere Discuss., doi:10.5194/tc-2016-88, 2016
Manuscript under review for journal The Cryosphere
Published: 27 April 2016




problems by applying the dynamic relaxation technique (Cundall, 1989) to Eq. (2), of which details are given below.

The temperature field of the ice is modeled using the following heat equation:

$$\rho c_p \dot{T} + \boldsymbol{v} \cdot \boldsymbol{\nabla T} = k \boldsymbol{\nabla^2 T}, \quad (3)$$

where $T$ is the temperature in Kelvin, $c_p$ is the heat capacity of ice, and $k$ is the thermal conductivity of ice. We do not include the effects of deformational strain heating within the ice. For the temperature field we impose Dirichlet boundary conditions on the ice surface and base, as well as at any water boundaries.

The governing equations are discretized using an unstructured mesh composed of triangular (2D) or tetrahedral (3D) elements. The approximate displacement $\boldsymbol{x}$, velocity $\boldsymbol{u}$, acceleration $\boldsymbol{a}$, force $\boldsymbol{f}$, and temperature $T$ are defined with linear basis functions (i.e., with P1 elements), while other physical quantities (e.g., stress $\boldsymbol{\sigma}$ and strain $\boldsymbol{\varepsilon}$) and material properties (e.g., density $\rho$ and viscosity $\eta$) are piecewise constant over elements. Conservation of mass is enforced via elasticity rather than the incompressibility condition. A general schematic of DES' solution scheme is shown in Fig. 1.

Boundary value problems must be complemented with appropriate boundary conditions to ensure that they are well-posed, and we present more detailed descriptions of these in the Section 3 where our simple experiments are described. In DES we make use of both stress and velocity boundary conditions. Subaerial ice is subject to a traction-free boundary condition, or $\boldsymbol{\sigma} \cdot \boldsymbol{n} = \boldsymbol{0}$. Floating ice is subject to a traction boundary condition as well, where the traction arises from applied normal stress equal to the weight of the water column displaced by the ice plus an additional, periodic tidal signal. This bottom boundary traction is uniformly applied to floating boundaries corresponding to 1 m of water displacement. As yet, the location of grounding lines are prescribed a priori in DES and do not evolve according to ice thickness or other environmental variables.

### 2.2 Numerical considerations

DES is formulated as an explicit finite element method, and the order of calculations can be seen in Fig. 1. The advantage of using this method is that the computational cost of each time step is small

The Cryosphere Discuss., doi:10.5194/tc-2016-88, 2016
Manuscript under review for journal The Cryosphere
Published: 27 April 2016




(compared to implicit methods where advancing by one large time step involves the solving of large, ill-conditioned linear systems) and the implementation of non-linear rheologies is simple.

The use of the explicit time integration means that the time step is limited to very small values, on the order of $\Delta X_{min}/u_{elastic}$ where $\Delta X_{min}$ is the smallest edge length of an element and $u_{elastic}$ is the elastic wave speed (from the Courant-Friederics-Lewy condition). We overcome this limitation using the mass scaling technique, of which details are given in [Choi et al., 2013]. Because DES employs a suite of constitutive relations, we also need to consider the constraints on the time step size associated with the dominating deformational mechanism. The time step in these simulations is chosen as the minimum between

$$\Delta t = \min\{\Delta t_{elastic}, \Delta t_{maxwell}\} \quad (4)$$

where

$$\Delta t_{elastic} = \Delta X_{min}/2c\, u_{char} \quad (5a)$$

$$\Delta t_{maxwell} = \eta_{min}/4G \quad (5b)$$

and $\Delta X_{min}$ is the mimimum element facet length in the mesh (which evolves dynamically during model run time), $c$ is the inertial scaling parameter related to the dynamic relaxation, $\Delta u_{char}$ is the characteristic advective speed, $\eta_{min}$ is the minimum allowable viscosity, and $G$ is the shear modulus. This scheme ensures that the dominating deformational mechanism is adequately resolved in time. As such the time steps in DES are on the order of seconds to hours, depending largely on mesh parameters and the characteristic speed of the simulation as determined by the phenomenon the user wishes to resolve.

In addition to the dynamic time-stepping routine, several other numerical techniques are employed that distinguish this model from implicit finite element schemes commonly used to solve FS systems. DES solves the dynamic momentum balance equation, Eq. (2), by damping the inertial forces at each time step, giving rise to the quasi-static (i.e., static with time-dependent boundary conditions) solution. Originally proposed by Cundall [1989], this variant of dynamic relaxation applies forces at each node in the domain opposing the direction of the node's velocity vector:

The Cryosphere Discuss., doi:10.5194/tc-2016-88, 2016
Manuscript under review for journal The Cryosphere
Published: 27 April 2016




$$m\boldsymbol{a_i} = (\boldsymbol{f_{damped}})_i = \boldsymbol{f_i} - \chi\, sgn\,(\boldsymbol{u_i})|\boldsymbol{f_i}| \quad (6)$$

where the subscript *i* denotes the *i*-th component of a vector and the *sgn*(*) denotes the signum function. $\chi$ is a user-supplied damping factor ($\chi = 0.8$ has been shown to ensure stability, e.g., Choi et al., 2013).

The linear triangular elements used in DES are known to suffer volumetric locking when subject to incompressible deformations (e.g., Hughes, 2000). Because we model phenomena that require incompressible plastic and viscous flow, we use an anti-volumetric-locking correction based on the nodal mixed discretization methodology (Detournay and Dzik, 2006; De Micheli and Mocellin, 2009). The technique simply averages the volumetric strain rate over a group of neighboring elements and then replaces each element's volumetric strain rate with the averaged one. Choi et al. [2013] describes this technique in greater detail.

Finally, DES makes use of adaptive remeshing. Based on the quality constraints selected by the user, DES assesses the mesh quality at fixed step intervals and remeshes if elements are found in violation (e.g., if a triangular element contains an angle smaller than some input threshold). New nodes may be inserted into the mesh (or old ones deleted) and the mesh topology can be changed through edge flipping. The nodes are provided to the Triangle library (Shewchuk, 1996) to construct a new triangulation of the domain. After the new mesh is created, the boundary conditions, derivatives of shape functions, and mass matrix are recalculated. When deformation is distributed over a large region or the whole domain, remeshing may result in a new mesh quite different from the old one. Because of this possibility the fields associated with nodes (e.g., velocity and temperature) are linearly interpolated from the old mesh to the new. For data associated with elements (e.g., strain and stress) DES uses an approximate conservative mapping described in detail by Ta et al. [2015].

## 3 Experiments: different constitutive models for ice

In Choi et al. [2013], DES performed the benchmark tests for a range of material or rheological behaviors to validate and verify this numerical method. These tests included: 1 – flexure of a finite-length elastic plate; 2 – thermal diffusion of a half-space cooling plate; 3 – stress build-up in a Maxwell viscoelastic material; 4 – Rayleigh-Taylor instability; and 5 – Mohr-Coulomb oedometer test. Thus

The Cryosphere Discuss., doi:10.5194/tc-2016-88, 2016
Manuscript under review for journal The Cryosphere
Published: 27 April 2016




DES has been verified and validated and is already in use in fields relating to crustal deformation (Ta et al., 2015). Indeed, any of these rheological choices may be employed to attempt the simulation of ice flow and failure. However, as we are interested in the effects that certain constitutive choices have on the time-dependent deformation of ice, we divide the this section according to how different constitutive models available within DES simulate the brittle, ductile, and semi-brittle (or mixed mode of ductile and brittle) deformation of ice.

### 3.1 Purely ductile or brittle ice

Observations have shown that the bending that occurs as ice transitions from resting on land to floating in water (an area termed the grounding line) promotes the failure of ice from the bottom up, called basal crevasses, that often appear with characteristic regularity in spacing, persisting within the ice for long distances and eventually promoting the calving of ice (Bindschadler et al., 2011; Glasser and Scambos, 2008; Logan et al., 2013; McGrath et al., 2012; James et al., 2014; Murray et al., 2014). In order to examine the effect that rheological assumptions have on the observed deformation field, we simulate an idealized version of this scenario where we test the effect that a forced bend has on a parallel-sided slab with either a purely brittle or ductile rheology (Fig. 2). The simplicity of this geometric setup allows us to examine the effect that bending has on ice approximated with either a purely ductile or brittle rheology, and to attribute differences between the two deformation patterns solely to the choice in rheology. For the simulation of brittle behavior we use an elastic stress update in DES with a Mohr-Coulomb failure envelope; for ductile behavior we approximate the rheology as a Maxwell viscoelastic solid, where the viscosity is determined by Glen's flow law (values taken from the literature and shown in Table 1, e.g., Larour et al., 2012):

$$\eta = \frac{1}{2} A^{-1/n} \dot{\varepsilon}_e^{(1-n)/n} \quad (6).$$

We set the ice thickness to 1000 m and prescribe the left, bottom, and right side velocities to be 300 m yr$^{-1}$, as these are realistic values for marine outlet glaciers. The initial mesh resolution is 50 m. The left and basal boundary velocities are tilted to an angle of 3 degrees for all horizontal positions $x$ in the domain less than 10 km, and are forced horizontal for $x$ greater than this location (the transition

The Cryosphere Discuss., doi:10.5194/tc-2016-88, 2016
Manuscript under review for journal The Cryosphere
Published: 27 April 2016




representing our idealized bending and 'grounding line'). The temperature of the ice is defined by a linear gradient between Dirichlet conditions of −30° C at the surface to 0° C at the base.

Figure 3 shows the effective stress (a), strain rate (c) and viscosity (e) after twenty years model time for purely brittle ice. Purely brittle ice experiences stress 1 to 2 orders of magnitude higher than purely ductile ice (Fig. 3b, d, f). For the brittle case, stresses are highest (about 1 MPa) on the basal surface and in a thin vertical line where the surface bends at the grounding line, whereas in the ductile ice case we observe only a slight increase in stress at the grounding line and nowhere else. Overall we observe in both experiments lower viscosity ice at the grounding line and higher ice viscosity upstream and downstream of the grounding line (Fig. 3e and f), however for the ductile case there is a much wider zone of low viscosity ice – by as much as 2 orders of magnitude smaller than the brittle ice. This means that the strains associated with deformation are more localized for the brittle rheology (limited to about 1 or 2 elements in width making for a very small deformational process zone) and conversely very diffuse for the ductile rheology. The comparative weakness and low effective viscosity of the ductile rheology is reflected by the surface topography: the left-hand side of the domain in the ductile simulation shows a steep depression at the ice surface, where the ice is essentially slumping toward the right-hand side of the domain under the force of gravity. The rather jagged shaped surface elsewhere in the domain is an artifact of low resolution and experiments performed with higher resolution saw these features disappear. Additionally, the velocity boundary condition imposed at the left side of the domain introduces an artifact in the flow that is expressed as an artificial steep surface depression: while the boundary nodes' velocities are prescribed, the nearby interior nodes relax and flow downhill under the force of gravity.

Because these simulations are intended to only compare ductile and brittle approximations for ice flow, the ductile ice does not fail (no yield envelope has been provided for this stress calculation). The brittle ice can and does fail, however, as dictated by the Mohr-Coulomb threshold, with a pattern shown in Fig. 4. Reasonable values for the yield envelope properties were selected from the literature and are listed in Table 1 (Bassis and Jacobs, 2013; Fish and Zaretsky, 1997; Sammonds et al., 1998). The plastic strain (or amount of strain a failed element undergoes once it has reached yield stress) for the brittle ice shows a very regular, localized pattern that is reminiscent of an idealized version of a field

The Cryosphere Discuss., doi:10.5194/tc-2016-88, 2016
Manuscript under review for journal The Cryosphere
Published: 27 April 2016




of basal crevasses (van der Veen, 1998; Bassis and Ma, 2015). We executed the same experiments with applied velocities of 600 and 900 m $yr^{-1}$ and saw no difference in the spacing or amount of strain. That is, failure patterns were insensitive to the speed at which the slab was advected down the slope and through the bend. During model simulation the strain begins at the base of the slab at the bending fulcrum (similar to the grounding line of a glacier) and quickly propagates upward toward the surface. Ice upstream of the grounding line remains fully intact until reaching the thin process zone delineated by the stress and strain rate fields shown in Fig. 3a and c. Once the ice has been advected away from this thin zone of high stress and strain rate the accumulation of post-failure strain ceases, leaving a pattern of regularly spaced, thin, vertical lines of failed ice, that have failed in sequence.

While this experiment shows that brittle ice deformation approximated through Mohr-Coulomb elasto-plasticity can model the evolution of fracture in a tilted, parallel-sided slab, it does not account for the expected flow due to the viscosity of the ice. In the following section we simulate a mixture of these two modes of deformation, brittle and ductile simultaneously, and show how brittle shear and tension fractures interact with ductile flow depending on stress and strain rate. We term this mixed ductile and brittle behavior as semi-brittle.

### 3.2 Semi-brittle behaviour

In computational mechanics, time-dependent semi-brittle behavior (a simultaneous mix of ductile and brittle deformation) is often simulated using damage theory (Pralong et al., 2003; Duddu et al., 2013; Krug et al, 2014, 2015; Borstad et al., 2016). In these recent models, stresses are approximated using viscoelasticity (Pralong et al., 2003; Duddu et al., 2013) or simply viscous friction (Borstad et al., 2016), and a calculation is carried throughout to determine a scalar damage variable that varies between 0 and 1 (0 for perfectly virgin ice, 1 for completely fractured). The theory relies on the assumption of recovery (via inversion) of a critical strain or strain-rate value after which ice begins to accumulate damage. Here we want to investigate the partitioning of viscous or ductile ice flow and brittle failure under boundary conditions that promote the formation of basal crevasses at glacier grounding lines – areas of fast ice movement and flexure. We suggest this represents an advance from previous damage-centric models where damage is estimated either in static snapshots throughout time (Borstad et al.,

The Cryosphere Discuss., doi:10.5194/tc-2016-88, 2016
Manuscript under review for journal The Cryosphere
Published: 27 April 2016




2016) for entire ice sheets or in completely time-dependent but small-strain conditions, as in Duddu et al., 2013 (i.e., the domain was not characterized by strains exceeding 100 % with advecting ice).

In glaciological literature there is evidence for a transition from ductile flow to brittle failure depending on the applied strain rate: specimens of ice experiencing low strain rate flow in a ductile manner, with viscosities adhering to Eq. 7, and those straining faster than a laboratory observed value of $10^{-7}$ $s^{-1}$ will fail in a brittle manner (Schulson and Duval, 2009, chapter 9). Simply following these observations: DES selects either the ductile or brittle constitutive update based on the local strain rate field (see the steps in the pseudo-code, Fig. 1). Elements in the domain with a strain rate less than $10^{-7}$ $s^{-1}$ are approximated as ductile (or Maxwell viscoelastic) and elements straining faster are approximated as brittle (or Mohr-Coulomb elasto-plastic). The semi-brittle rheology employed here is supported by laboratory data that show that a stiffening of ice at a high strain rate will be accompanied by fracture only at correspondingly high tensile stress (from $10^5$ to $10^6$ Pa) (Bassis and Jacobs, 2013; Schulson and Duval, 2009). The strain rate dependent nature of the transition from ductile to brittle implies that – depending on the viscosity – fracture in ice occurs on time scales of less than a few seconds to hours, which DES easily resolves.

In an effort to simulate a more realistic glacier grounding line we initialize this experiment with a horizontal wedge of ice: the gradient in ice thickness drives ice flow entirely. In this setup (Fig. 2b) we maintain a static grounding line, and due to numerical constraints on DES' remeshing algorithm, we cannot maintain the initial thickness gradient; thus, the driving stress decreases throughout the simulation, leading to a model time of approximately 3 years. We believe the initial and boundary conditions represent a sufficient next step toward a more realistic simulation as the ice flow is generated more realistically by a gradient in ice thickness and we employ a jump in boundary conditions (from velocity to represent bedrock conditions to stress representing floatation) at the grounding line, and are confident that choices made in model initialization allow us to focus on results that reflect the more complicated and dynamic rheology we wish to examine. The geometry of the domain is shown in Fig. 2b, where the thickness of the left side is 1050 m, decreasing linearly over 50 km to 900 m on the right. We found that this initial thickness gradient produces a driving stress with reasonable terminus velocities matching to those of glaciers with ice shelves in Antarctica (Rignot et al., 2011). We

The Cryosphere Discuss., doi:10.5194/tc-2016-88, 2016
Manuscript under review for journal The Cryosphere
Published: 27 April 2016




employed a different setup previously (to examine purely brittle or ductile rheology) because purely brittle ice initialized as shown in Fig. 2b does not flow; it remains static.

We apply a bending moment in the ice at the grounding line with a jump in boundary conditions from freely slipping (where the horizontal velocity is free but the vertical is forced equal to 0) on the grounded, bedrock supported ice to freely floating at 48 km in the horizontal direction. To the right of 48 km the ice is subject to a stress boundary condition with two components: a floatation condition that applies a force equal to the weight of the water column displaced by ice below sea level, and a periodic, tidal force that corresponds to a 1 m diurnal tidal deflection. No ice melting is applied to these boundaries as this effect is the subject of future work.

Figure 5 shows the velocity, effective stress, strain rate, and viscosity at 6 months model time. Up until this time in the simulation the ice reaches a maximum velocity of about 2 km $a^{-1}$, after which the velocities decrease to 0 due to a loss of driving stress as the ice extends into the floating portion of the domain. Stresses at the grounding line in these simulations are high: about 1 MPa at the grounding line, similar to the behavior we saw in previous experiments (Fig. 3).

We also determine the distribution of ice failure for the semi-brittle rheology (Fig. 6). Ice at the surface is regularly and heavily broken as the yield strength there is the lowest (this is the case for all frictional materials in the vertical plane). As the floating portion of the ice extends further past the grounding line the ice thins, allowing for necking at the grounding line and other places the ice has failed in the floating tongue. This thinning as ice begins to float is a feature of marine-terminating ice sheets, and is accentuated in nature by intense basal melting. Toward the end of the simulation the floating tongue has accumulated so much strain that it begins to form undulated pinch-and-swell structures (Fig. 6), very much like those see on Pine Island and Thwaites Glaciers (Bindschadler et al., 2011; Logan et al., 2013). We term this characteristic pinch-and-swell geometry boudins, where we count 18 boudins that have a mean spacing of 530 m and a standard deviation of 150 m. While the basal crevasses form sequentially, that is – failed ice to the right of the domain are older than those to the left – these features develop more fully into the characteristic boudin-like shape all at the same time in the

The Cryosphere Discuss., doi:10.5194/tc-2016-88, 2016
Manuscript under review for journal The Cryosphere
Published: 27 April 2016




model. Once the ice has lost all its driving stress the ice begins to thicken just beyond the grounding line, which is a consequence of the boundary conditions and the lack of true bedrock below the ice.

## 4 Discussion and conclusion

The experiments performed in this study are not meant to be exhaustive and wide-reaching; rather, they were performed to show how a semi-brittle ice-like material responds to very idealized initial and boundary conditions. Because we do not actually simulate fractures – ice in DES is represented as a continuum material – we must assume that at some level of plastic strain, the ice in a simulation is considered broken. Zones of intense, vertical localization in these experiments can be considered to have ruptured and further, in essence, could represent basal crevasses. These 'crevasses' initiate in virgin material where the shear and extensional stresses due to bending and increases in velocity are highest and are then advected downstream from the grounding line. As this work represents an initial exploration and presentation of the model's capability, simulations with more realistic boundary conditions and explorations of how those boundary conditions affect the pattern of ice failure are left for later studies. For example, the loss of driving stress in the semi-brittle experiment could be mitigated by applying a velocity condition on the left boundary, or simply by remeshing the left side geometry to its original shape. Our focus here truly is on the effect of rheological choices, and with this goal in mind we have tried to design experiments idealized enough so that differences in deformation can truly be attributed to rheology. Similarly, while our simulations are carried out under the condition of conservation of energy, we do not explore the effect of changing ice temperature on ice flow; rather, we carry out the experiments under this condition to demonstrate that future experiments will be able to solve both conservation of momentum (with non-zero acceleration) and energy without too much computational cost. Indeed, the simulations presented here have all been computationally cheap – with the largest domain in the semi-brittle experiments being carried out on 4 cores in 1 hour.

From very simple model runs we learned there may indeed be a ductile to brittle transition in ice that is likely very difficult to capture in many numerical models. Bassis and Jacobs [2013] recently modeled the retreat of Helheim glacier using tightly packed particles that interacted elastically and

The Cryosphere Discuss., doi:10.5194/tc-2016-88, 2016
Manuscript under review for journal The Cryosphere
Published: 27 April 2016




broke once a threshold stress was achieved, often due to the influences of basal topography and buoyancy in floating portions. We aimed to extend their work by including the effect of viscous stresses on ice deformation. Figure 7 indicates how we imagine failure and subsequent deformation occurs in floating ice masses in nature: at grounding lines, both an increase in ice velocity (due to loss of retaining frictional forces applied by bedrock contact) and an application of bending moment (due to tides and the equilibrated response beams and plates exhibit when they are partially supported by fluid) lead to high stresses and strain rates that initiate ice failure from the bottom up (Fig. 7a). As ice accelerates into open ocean it thins, promoting further crack propagation, which can be further widened by intrusions of warm, buoyant melt water (Fig. 7b). Further, thinning, stretching, and ice melting when simulated with a semi-brittle rheology like the one presented here leads to ice geometries that are like those seen in nature (Bindschadler et al., 2011; Luckman et al., 2012). Since the location and size of basal crevasses can directly impact calving rates by propagating upward through the full thickness of the ice (Logan et al., 2013) understanding their evolution and growth may be critical to predicting calving occurrence and terminus position.

Future work with DES will explore the utility of a semi-brittle ice rheology in more realistic scenarios and with the inclusion of a freely varying grounding line (i.e., one that evolves based on ice thickness) and basal melting – two ice dynamic processes incorporated in other numerical models and known to be critical processes in glacier and ice sheet retreat. At present this study has shown that the assumption of a semi-brittle ice rheology can reproduce the brittle rupture of ice, general ice flow characteristics, and idealized patterns of failure in simple situations, and can be recommended as a tool through which future studies of ice failure related to calving and ice dynamics can be conducted.

**Author contributions**

L. Logan, L. Lavier, and G. Catania helped design the experiments performed herein. L. Logan coded and executed these experiments, and prepared this manuscript. E. Choi and E. Tan developed the code in large part, which was modified by L. Logan and L. Lavier for the experiments in this paper.



**Acknowledgements**

This work was funded by NSF grant ARC-0941678 and the King Abdullah University of Science and Technology. The ice modeling was performed at the University of Texas, Institute for Geophysics; the University of Memphis; and Academia Sinica in Taiwan. The authors gratefully acknowledge A. Vieli, who provided helpful comments.

**References**

Amundson, J. M. and Truffer, M.: A unifying framework for iceberg-calving models, Journal of Glaciology, 56(199), 1–9, 2010.

Bassis, J. N.: Diverse calving patterns linked to glacier geometry, Nature Geoscience, 6(10), 833–836, doi:10.1038/ngeo1887, 2013.

Bassis, J. N. and Ma, Y.: Evolution of basal crevasses links ice shelf stability to ocean forcing, Earth and Planetary Science Letters, 409(C), 203–211, doi:10.1016/j.epsl.2014.11.003, 2015.

Bassis, J. N., Fricker, H. A., Coleman, R. and Minster, J.-B.: An investigation into the forces that drive ice-shelf rift propagation on the Amery Ice Shelf, East Antarctica, Journal of Glaciology, 54(184), 1–11, 2008.

Bindschadler, R. A., Vaughan, D. G. and Vornberger, P.: Variability of basal melt beneath the Pine Island Glacier ice shelf, West Antarctica, Journal of Glaciology, 57(2004), 1–15, 2011.

Borstad, C., Khazendar, A., Scheuchl, B., Morlighem, M., Larour, E. and Rignot, E.: A constitutive framework for predicting weakening and reduced buttressing of ice shelves based on observations of the progressive deterioration of the remnant Larsen B Ice Shelf, Geophys. Res. Lett., 43(5), 2027–2035, doi:10.1002/2015GL067365, 2016.

Budd, W. F. and Jacka, T. H.: A review of ice rheology for ice sheet modelling, Cold Regions Science and Technology, 16, 107–144, 1989.

Choi, E., Tan, E., Lavier, L. L. and Calo, V. M.: DynEarthSol2D: An efficient unstructured finite element method to study long-term tectonic deformation, J. Geophys. Res. Solid Earth, 118(5), 2429–2444, doi:10.1002/jgrb.50148, 2013.

Cundall, P. A.: Numerical experiments on localization in frictional materials, *Ing. Arch.*, *58*, 148 – 159, 1989.

De Micheli, P. O., and Mocellin, K.: A new efficient explicit formulation for linear tetrahedral elements non-sensitive to volumetric locking for infinitesimal elasticity and inelasticity, *Int. J. Numer. Methods Eng.*, *79*, 45 – 68, doi: 10.1002/nme.2539, 2009.

Detournay, C., and Dzik, E.: Nodal mixed discretization for tetrahedral elements, in *4th International FLAC Symposium on Numerical Modeling in Geomechanics*, edited by Hart, and Varona, col. C, Itasca Consulting Group, Inc., Minneapolis, 2006.

Duddu, R. and Waisman, H.: A temperature dependent creep damage model for polycrystalline ice, Mechanics of Materials, 46, 23–41, doi:10.1016/j.mechmat.2011.11.007, 2012.

Duddu, R., Bassis, J. N. and Waisman, H.: A numerical investigation of surface crevasse propagation in glaciers using nonlocal continuum damage mechanics, Geophys. Res. Lett., 40(12), 3064–3068, doi:10.1002/grl.50602, 2013.

Fish, A. M. and Zaretsky, Y. K.: Strength and creep of ice in terms of Mohr-Coulomb fracture theory, Proceedings of International Offshore and Polar Engineering Conference, 2, 1–9, 1998.

Gagliardini, O. and Zwinger, T.: The ISMIP-HOM benchmark experiments performed using the Finite-Element code Elmer, The Cryosphere, 2, 67–76, 2008.

Glasser, N. F. and Scambos, T. A.: A structural glaciological analysis of the 2002 Larsen B ice-shelf collapse, Journal of Glaciology, 54(194), 1–14, 2008.

Glen, J. W.: The Creep of Polycrystalline Ice, Proceedings of the Royal Society A: Mathematical, Physical and Engineering Sciences, 228(1175), 519–538, doi:10.1098/rspa.1955.0066, 1955.

Goldsby, D. L. and Kohlstedt, D. L.: Superplastic deformation of ice: Experimental observations, J. Geophys. Res., 106(B6), 11017–11030, 2001.

Hughes, T. J.: *The Finite Element Method: Linear Static and Dynamic Finite Element Analysis*, 672 pp., Dover Publication, reprint of the Prentice-Hall, Inc., Englewood Cliffs, New Jersey, 1987 edition, 2000.

James, T. D., Murray, T., Selmes, N., Scharrer, K. and O'Leary, M.: Buoyant flexure and basal crevassing in dynamic mass loss at Helheim Glacier, Nature Geosci, 7(8), 593–596, doi:10.1038/ngeo2204, 2014.

Krug, J., Weiss, J., Gagliardini, O., and Durand, G.: Combining damage and fracture mechanics to model calving, The Cryosphere, 8, 2101-2117, doi:10.5194/tc-8-2101-2014, 2014.

Krug, J., Durand, G., Gagliardini, O., and Weiss, J.: Modelling the impact of submarine frontal melting and ice melange on glacier dynamics, The Cryosphere, 9, 989-1003, doi:10.5194/tc-9-989-2015, 2015.

Larour, E., Seroussi, H., Morlighem, M. and Rignot, E.: Continental scale, high order, high spatial resolution, ice sheet modeling using the Ice Sheet System Model (ISSM), J. Geophys. Res., 117(F1), n/a–n/a, doi:10.1029/2011JF002140, 2012.

Levermann, A., Albrecht, T., Winkelmann, R., Martin, M. A., Haseloff, M. and Joughin, I.: Kinematic first-order calving law implies potential for abrupt ice-shelf retreat, The Cryosphere, 6(2), 273–286, doi:10.5194/tc-6-273-2012, 2012.

Lipscomb, W. H., Fyke, J. G., Vizcaíno, M., Sacks, W. J., Wolfe, J., Vertenstein, M., Craig, A., Kluzek, E. and Lawrence, D. M.: Implementation and Initial Evaluation of the Glimmer Community Ice Sheet Model in the Community Earth System Model, J. Climate, 26(19), 7352–7371, doi:10.1175/JCLI-D-12-00557.1, 2013.

Logan, L., Catania, G., Lavier, L. and Choi, E.: A novel method for predicting fracture in floating ice, Journal of Glaciology, 59(216), 750–758, doi:10.3189/2013JoG12J210, 2013.

Luckman, A., Jansen, D., Kulessa, B., King, E.C., Sammonds, P. and Benn, D.I.: (2012) Basal crevasses in Larsen C Ice Shelf and implications for their global abundance. Cryosphere, 6(1), 113–123, doi: 10.5194/tc-6-113-2012.

MacAyeal, D. R. and Sergienko, O. V.: The flexural dynamics of melting ice shelves, Annals of Glaciology, 54(63), 1–10, doi:10.3189/2013AoG63A256, 2013.

Mahrenholtz, O. and Wu, Z.: Determination of creep damage parameters for polycrystalline ice, Advances in Ice Technology, 181–192, 1992.

Martin, C., Navarro, F., Otero, J., Cuadrado, M. L. and Corcuera, M. I.: Three-dimensional modelling of the dynamics of Johnsons Glacier, Livingston Island, Antarctica, Annals of Glaciology, 39, 1–8, 2004.

McGrath, D., Steffen, K., Rajaram, H., Scambos, T., Abdalati, W. and Rignot, E.: Basal crevasses on the Larsen C Ice Shelf, Antarctica: Implications for meltwater ponding and hydrofracture, Geophys. Res. Lett., 39(16), n/a–n/a, doi:10.1029/2012GL052413, 2012.

P R Sammonds, S. A. F. Murrell, and M. A. Rist: Fracture of multiyear sea ice,, 1–21, 2015.

Pralong, A., Funk, M. and Lüthi, M. P.: A description of crevasse formation using continuum damage mechanics, Annals of Glaciology, 37, 1–6, 2003.

Rignot, E., Mouginot, J. and Scheuchl, B.: Ice Flow of the Antarctic Ice Sheet, Science, 333(6048), 1427–1430, doi:10.1126/science.1208336, 2011.

Schulson, E.M., and Duval, P.: (2009) *Creep and fracture of ice.* Cambridge University Press, Cambridge.

Shewchuk, J.: Triangle: Engineering a 2D quality mesh generator and Delaunay triangulator, in *Applied Computational Geometry: Towards Geometric Engineering, Lecture Notes in Computer Science,* edited by M. C. Lin, and D. Manocha, pp. 203 – 222, vol. 1148, Springer-Verlag, Berlin, 1996.

Ta, T., Choo, K., Tan, E., Jang, B. and Choi, E.: Accelerating DynEarthSol3D on tightly coupled CPU–GPU heterogeneous processors, Computers and Geosciences, 79(C), 27–37, doi:10.1016/j.cageo.2015.03.003, 2015.

Tavi Murray, N. Selmes, T. D. James, S. Edwards, I. Martin, T. O'Farrell, R. Aspey, I. Rutt, M. Nettles, T. Bauge: Dynamics of glacier calving at the ungrounded margin of Helheim Glacier, southeast Greenland,, 1–19, doi:10.1002/(ISSN)2169-9011, 2015.

van der Veen, C. J.: Fracture mechanics approach to penetration of surface crevasses on glaciers, Cold Regions Science and Technology, 27, 31–47, 1998.

Weiss, J.: Subcritical crack propagation as a mechanism of crevasse formation and iceberg calving, Journal of Glaciology, 50(169), 1–7, 2004.

Winkelmann, R., Martin, M. A., Haseloff, M., Albrecht, T., Bueler, E., Khroulev, C. and Levermann, A.: The Potsdam Parallel Ice Sheet Model (PISM-PIK) – Part 1: Model description, The Cryosphere, 5(3), 715–726, doi:10.5194/tc-5-715-2011, 2011.

The Cryosphere Discuss., doi:10.5194/tc-2016-88, 2016
Manuscript under review for journal The Cryosphere
Published: 27 April 2016




| *Symbol* | *Constant* | *Value* | *Units* |
|---|---|---|---|
| $\rho$ | Density of ice | 911 | kg $m^{-3}$ |
| $n$ | Power in Glen's Law | 3 | - |
| $A$ | Multiplier in Paterson and Budd (1982) | | |
| | if T < 263 K | $3.615 \times 10^{-13}$ | $s^{-1}$ $Pa^{-3}$ |
| | if T ≥ 263 K | $1.733 \times 10^{3}$ | $s^{-1}$ $Pa^{-3}$ |
| $Q$ | Activation energy for creep in Paterson and Budd (1982) | | |
| | if T < 263 | $6 \times 10^{4}$ | J $mol^{-1}$ |
| | if T ≥ 263 K | $13.9 \times 10^{4}$ | J $mol^{-1}$ |
| $\sigma_T$ | Strength in tension | 1 | MPa |
| $\boldsymbol{\phi}$ | Angle of internal friction | $30^{o}$ | |
| $C$ | Cohesion | .1 | MPa |
| $K$ | Bulk modulus | 9500 | MPa |
| $c_p$ | Heat capacity | 2000 | J $kg^{-1}$ $K^{-1}$ |
| $k$ | Thermal conductivity | 2.1 | W $m^{-1}$ $K^{-1}$ |

**Table 1: Parameters used in model runs whose values remained constant.**

The Cryosphere Discuss., doi:10.5194/tc-2016-88, 2016
Manuscript under review for journal The Cryosphere
Published: 27 April 2016




INITIALIZE. Supply list of boundary nodes, areas, holes, and facets to mesh library
FOR each time step *n*

Evaluate force at ith node — $\Sigma F_i = m_i a_i$
Get new velocities and displacements — $v_i = dt * a_i$, $x_i = dt * v_i$
Evalutate effective strain rate at each element — $E_{II} = sqrt(\dot{\varepsilon}_{ij}\dot{\varepsilon}_{ij})$

IF $E_{II}$ < threshold
Stress is ductile := Maxwell viscoelastic constitutive law — $\sigma_D = F(\varepsilon, \dot{\varepsilon}, T, ...)$
Else
Stress is brittle := Mohr-Coulomb elastoplastic constitutive law — $\sigma_B = G(\varepsilon, \dot{\varepsilon}, T, ...)$

Evaluate new forces from stress and local element area — $dF_i = 3 * \sigma_e d\Omega_e$

Evaluate mesh quality and remesh as necessary
END

**Figure 1: Schematic of one time step in DES.**

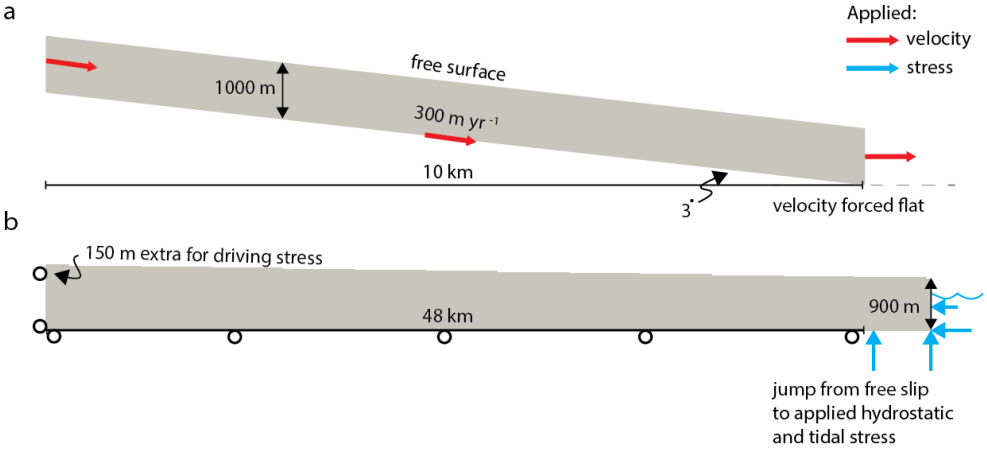


**Figure 2: Schematic of experiments. (a) Experiments performed with a purely ductile or brittle rheology are initialized as a parallel-sided slab that is advected down a plane and forced flat at 10 km. (b) Setup for semi-brittle rheology: a horizontal domain of 50 km and a fixed grounding line at 48 km, with an initial 2 km of floating tongue. The left-hand side horizontal velocity is fixed at zero and the bottom side upstream (left) of the grounding line vertical velocity is fixed at zero (this type of boundary condition is represented schematically by open black circles). Hyrdrostatic and tidal stress is applied to the bottom and right-hand side of the domain downstream (right) of the grounding line.**

The Cryosphere Discuss., doi:10.5194/tc-2016-88, 2016
Manuscript under review for journal The Cryosphere
Published: 27 April 2016


The Cryosphere Discussions
Open Access
EGU

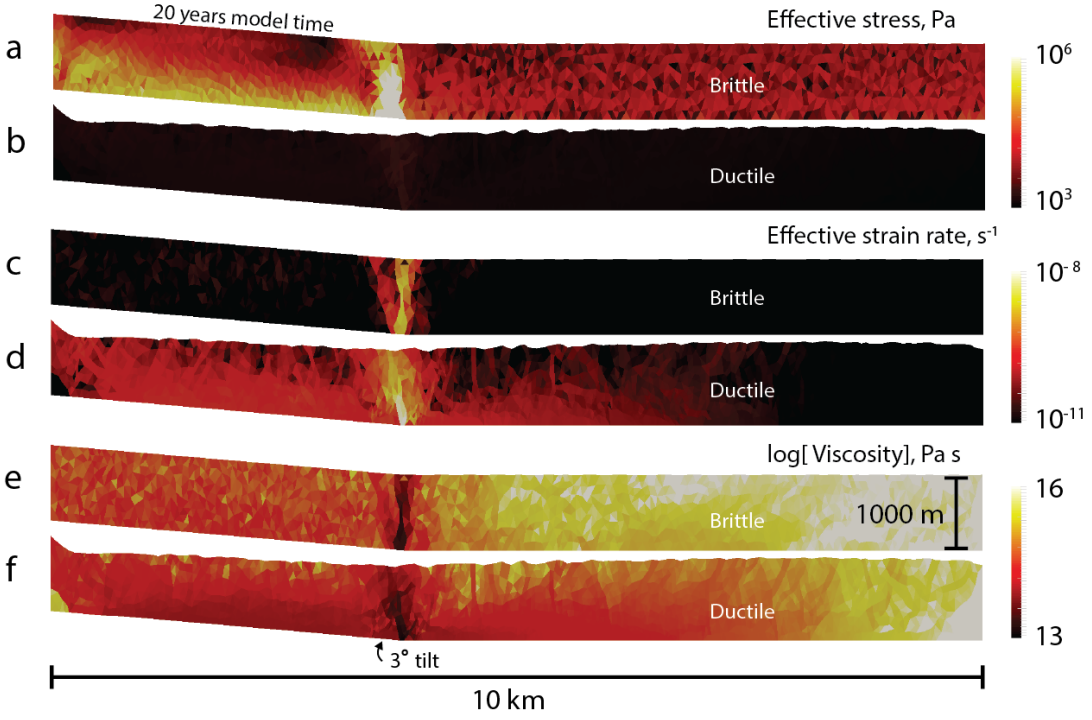


**Figure 3: Comparisons of purely brittle (a, c, e) and purely ductile (b, d, f) tilted slab experiments. (a, b) Effective stress, (c, d) effective strain rate, (e, f) viscosity after 20 years model time. While the boundary nodes are given prescribed velocities, the interior and surface nodes move freely; in the purely ductile case this results in the surface depression seen on the left side. The left boundary nodes are effectively pinned by the prescribed velocity but the ice slumps downhill due to gravity. The rather rough surface (most pronounced in the ductile case, though still present in the brittle case) is an artifact of low resolution that disappears in experiments with higher resolution.Overall the brittle rheology results in a narrow process zone of high stress and deformation, while the ductile rheology has a more diffuse area of strain and lower stresses.**

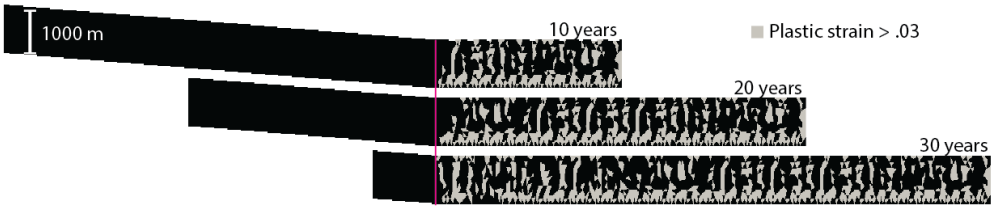


**Figure 4: Simulation of brittle ice slab being advected down the inclined plane throughout the model time. Pink vertical line denotes the change in the angle of applied velocity boundary conditions from 3 degrees to flat. Black ice indicates completely intact ice, while grey represents ice that has failed. Grey vertical lines appear with regularity, representing an idealized version of a field of basal crevasses in a glacier.**

The Cryosphere Discuss., doi:10.5194/tc-2016-88, 2016
Manuscript under review for journal The Cryosphere
Published: 27 April 2016


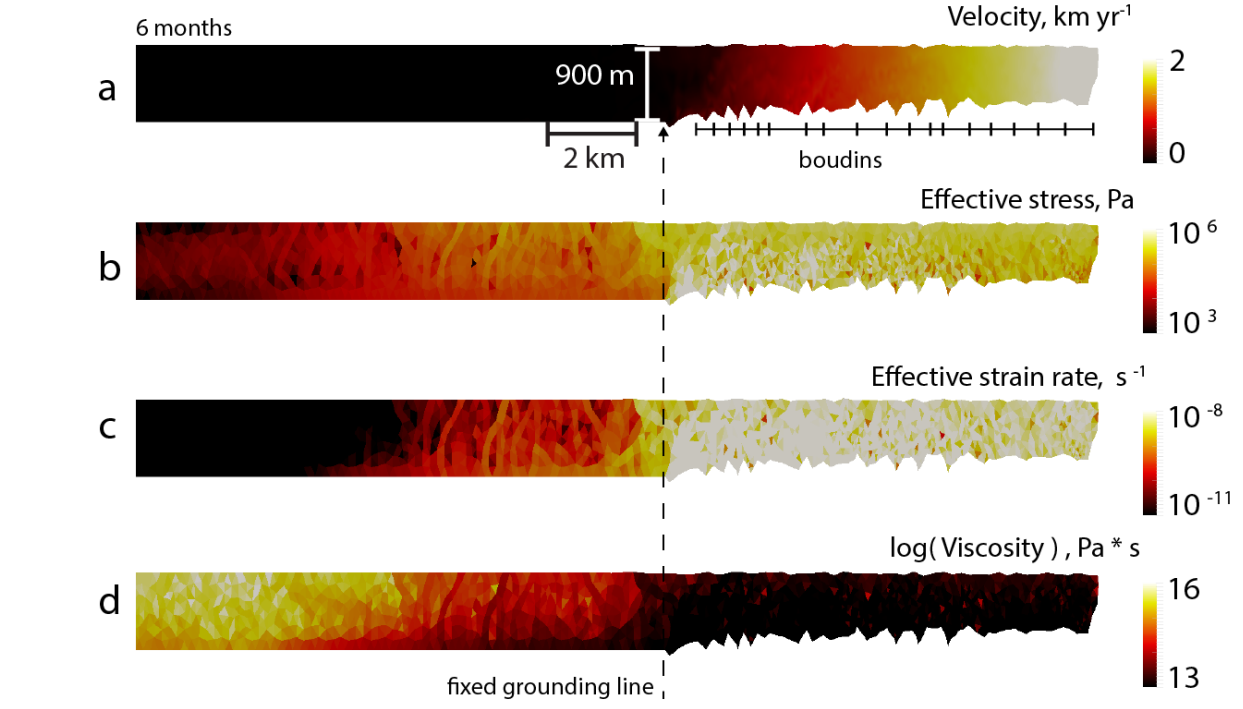


**Figure 5: Simulation of semi-brittle wedge of ice after 6 months model time, undergoing a jump in boundary conditions from freely slipping on the basal side (left of grounding line – dashed arrow) to floating in the ocean (right of grounding line). The horizontal velocity (a) is fixed at x = 0 and free elsewhere, while the vertical velocity is free at x = 0 and fixed to zero up to the grounding line. The gradient in thickness drives the flow of ice over the grounding line where ice experiences a transition to stress boundary conditions that represent floatation and 1 m tides. Dashed bars in the floating tongue show the development of boudins. The effective stress (b) and strain rate (c) fields both show orders of magnitude increases at the grounding line: the jump in strain rate allows the ice to be evaluated as brittle in DES and the associated stresses are high enough to reach yield (see Fig. 6). The corresponding viscosities (d) just upstream of the grounding line are high and decrease 3 orders of magnitude as the ice expands out into the ocean under its own weight.**

The Cryosphere Discuss., doi:10.5194/tc-2016-88, 2016
Manuscript under review for journal The Cryosphere
Published: 27 April 2016




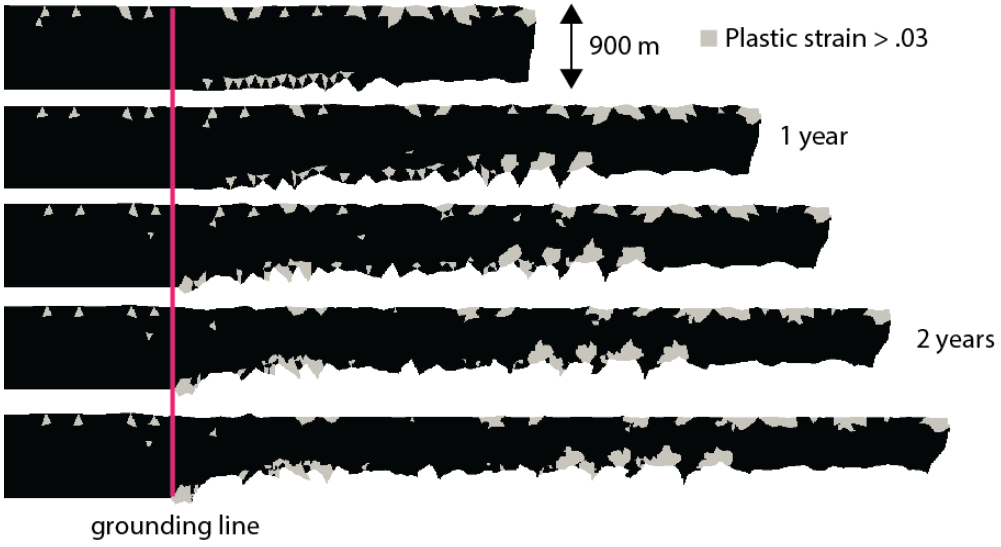


**Figure 6: Plastic strain over 2.5 years model time. Ice fails in tension at the surface near the terminus with regularity at the grounding line where hydrostatic stress is applied (in pink). Ice forms boudin-like features after accommodating a large amount of strain.**

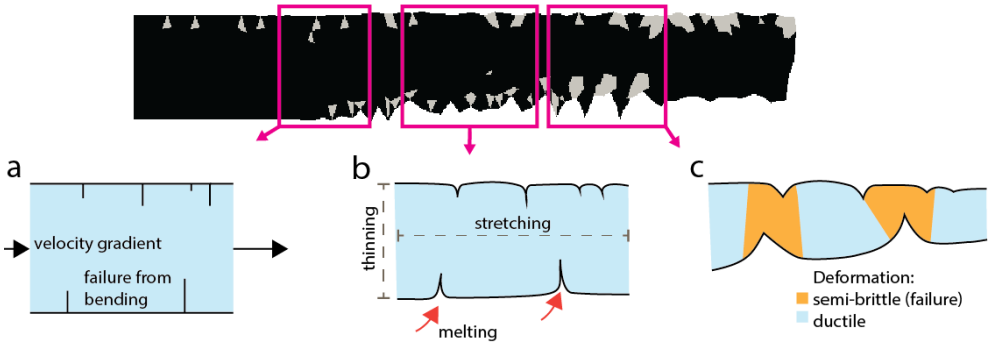


**Figure 7: Schematic of how semi-brittle deformation could proceed in nature, through space and time. (a) Initial failure forms due to high strain rates as ice accelerates across the grounding line, with the added bending due to tidal motion. (b) Ice continues to accelerate as it floats without resistance into the ocean; (not simulated here) melting from hot, buoyant water enters cracks and erodes crack walls, widening and thinning the ice. (c) Ice reaching its terminal speed at the front undergoes both semi-brittle deformation and ductile deformation. Semi-brittle failure occurs where ice has previously failed (in thin spots) and further thins the floating tongue, while ice between surface cracks and bottom cracks undergoes ductile deformation. The geometry produced by these processes resembles boudins, which eventually calve into the ocean.**